

Guy Carpenter Asia-Pacific Climate Impact Centre

Annual Report 2015



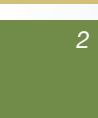
香港城市大學
City University of Hong Kong

Executive Summary

This is the seventh annual report issued by the Guy Carpenter Asia-Pacific Climate Impact Centre and covers the activities of the Centre in 2015. During the year, we continued to work on improving our understanding of the physical processes responsible for different types of climate variability in our region, which included winter monsoon in East Asia and urban heat island problems in Hong Kong. In the area of typhoons, a major focus was on tropical cyclone landfalling activity in East Asia, both of its decadal variation and seasonal forecast. We have been making efforts to improve air pollution measurements and expand their application. The effect of atmospheric circulations on local air quality was also investigated.

The report is divided into three sections, with a total of 15 projects. Section A focuses on climate variability of winter monsoon affecting East Asia, including indices representing its variability, characteristics of East Asian trough and winter moisture supply, as well as urban heat island problem in Hong Kong, including statistical analysis and possible cooling method. Section B contains studies examining variations of tropical cyclone landfalling activity along the East Asia coast and a summary of seasonal forecast of that activity in 2015. Section C reports on studies related to measurements of various pollutant species and development of an air monitoring system employed in an international sport event, as well as studies related to effect of atmospheric circulations on air quality and visibility in Hong Kong.

As in the past, the main results from each of the projects are briefly described in this report. The papers produced from these projects are available either from the CD attached to the report or from our website.



Contents

1 Executive Summary

5 I. Introduction

5 II. Research Projects

A. Climate Variability

- A1. *Simple metrics for representing East Asian winter monsoon variability*
- A2. *East Asian trough associated with East Asian winter monsoon*
- A3. *Winter moisture supply over Southwest China*
- A4. *Urban heat islands in Hong Kong: Statistical modeling and trend detection*
- A5. *Multi-purpose rainwater harvesting for water resource recovery and the cooling effect*
- A6. *Effect of sea surface temperature on local air temperature under high-resolution urban-canopy WRF in Hong Kong*

B. Tropical Cyclone

- B1. *Decadal change of tropical cyclone landfall latitude along the East Asia coast*
- B2. *Summary of 2015 seasonal forecasts of tropical cyclone activity in East Asia*
- B3. *Change in destructiveness of landfalling tropical cyclones over China*

C. Air Quality

- C1. *Speciation of water soluble iron with a novel dispersive absorption spectroscopic measurement technique*
- C2. *Development and application of a next generation air sensor network*
- C3. *Evaluation of diesel fleet emissions and control policies from plume chasing measurements of on-road vehicles*
- C4. *Top-down emission inventory development for fine resolution simulation*
- C5. *Synoptic weather control of summer air quality in Hong Kong*
- C6. *Intraseasonal variation of visibility in Hong Kong*

26 Publications

28 Staff List



I. Introduction

The Guy Carpenter Asia-Pacific Climate Impact Centre was established in June 2008. Since 2009, we have been issuing an annual report that describes our research activities during the year, and this is our seventh annual report that describes the activities of the Centre in 2015. During the year, we continued to work on climate problems related to Hong Kong, the Asia-Pacific region as well as those on a global scale, with a total of 15 projects. For each project, we summarise the main results for the reader to have a quick introduction of the subject. In most cases, the results have been published in one or more journal articles, which are listed at the end of the summary of each project. A copy of each of the publications is included in the CD attached to the report and is also available online at <http://www.cityu.edu.hk/gcacic/publications.htm>.

We hope that this report will provide the reader of an overall picture of the research activities of the Centre. Suggestions and comments on the projects are most welcome.

II. Research Projects

A. Climate Variability

A1. Simple metrics for representing East Asian winter monsoon variability

(PI: Wen ZHOU)

The Urals blocking pattern index (UBI) is found to be closely related to the cold air advection from the high latitudes towards western Siberia and shows an implicit linkage with the Siberian high intensity and the surface air temperature (SAT) variations north of 40°N in the East Asian winter monsoon (EAWM) region. Also, the western Pacific teleconnection index (WPI) is connected with the meridional displacement of the East Asian jet stream and the East Asian trough. This is strongly related to the SAT variations in the coastal area south of 40°N in the EAWM region. These relationships are equally strong on both interannual and interdecadal timescales (Figure 1). For more details, please refer to Cheung and Zhou (2016).

Two large-scale teleconnection patterns (Urals blocking pattern index and western Pacific teleconnection index) are used to represent the long-term variations in the East Asian winter monsoon.

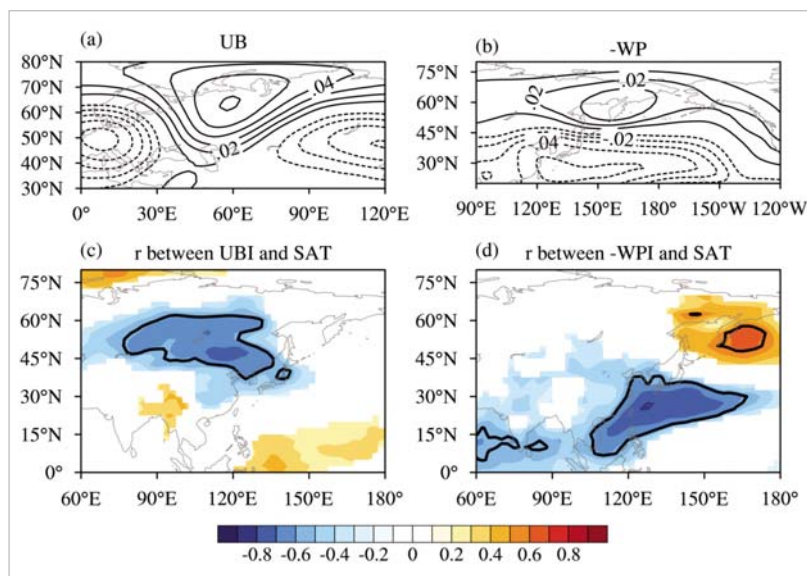


Figure 1. Eigenvector of the (a) Urals blocking (UB) and (b) western Pacific (WP) teleconnection patterns. Linear correlation coefficients between SAT and the principal component of (c) UB and (d) WP. In (c, d), only the regions significant at the 95% confidence level are shaded, and the values larger than 0.574 in magnitude (equivalent to one-third of the explained variance) are enclosed by thick contours.

Reference:

Cheung, H. H. N. and W. Zhou, 2016: Simple metrics for representing East Asian winter monsoon variability: Urals blocking and western Pacific teleconnection patterns. *Advances in Atmospheric Sciences*, 33, 708–718, doi: 10.1007/s00376-015-5204-6.

A2. East Asian trough associated with East Asian winter monsoon

(PI: Wen ZHOU)

During boreal winters, an anomalous cyclonic flow is likely to occur over the mid-latitude western North Pacific when the East Asian trough (EAT) is displaced southward. The cyclonic flow transports the cold air from northeast Asia southward and results in a colder-than-normal Southeast Asia. The situation is generally reversed when the EAT is displaced northward. On the other hand, the northeast Asian temperature is related to the strength and the east-west displacement of the EAT. A colder-than-normal northeast Asia is associated with a stronger-than-normal and a westward-displaced EAT. These three characteristics of the EAT account for around 50% of the temperature variation over the East Asian winter monsoon (Figure 2). For more details, please refer to Leung and Zhou (2015a).

This study examines different spatio-temporal characteristics of the East Asian trough (EAT), which includes its strength, its east-west and north-south displacements. The intraseasonal strength of the EAT is subjected to the downstream development of a stationary wave train across the Eurasian continent.

A persistent southward intrusion of cold air from the high-latitude East Asia to the mid-latitude East Asia is associated with the development of a strong EAT. Such an intrusion is controlled mainly by the temperature variation on intraseasonal timescales (10 to 89 days). On the other hand, the seasonal eddies (> 90 days) controls the north-westerly wind over the mid-latitude East Asia (Figure 3). For more details, please refer to Leung and Zhou (2015b).

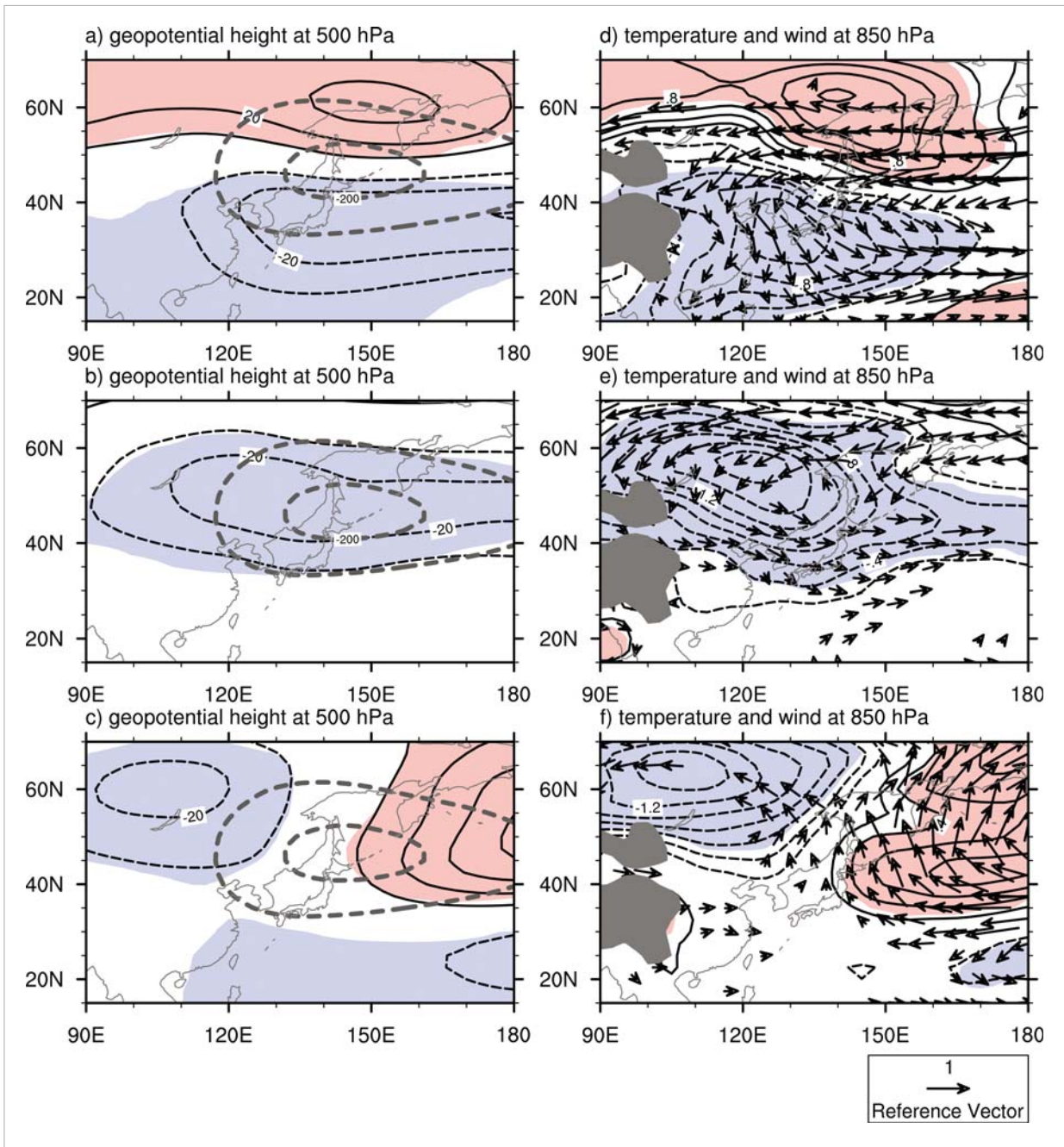


Figure 2. The regressions of geopotential height at 500 hPa (black contour; unit: m) onto the time series of (a) north-south displacement, (b) strength, and (c) east-west displacement. (d) to (f) are similar to (a) to (c), but for the horizontal wind (vector; unit: ms^{-1}) and temperature (shading; unit: K). The thick grey contours shows the climatology of eddy geopotential height at levels of -100 and -200 m. Red (blue) shading represents the positive (negative) contour values excess 5% significance level.

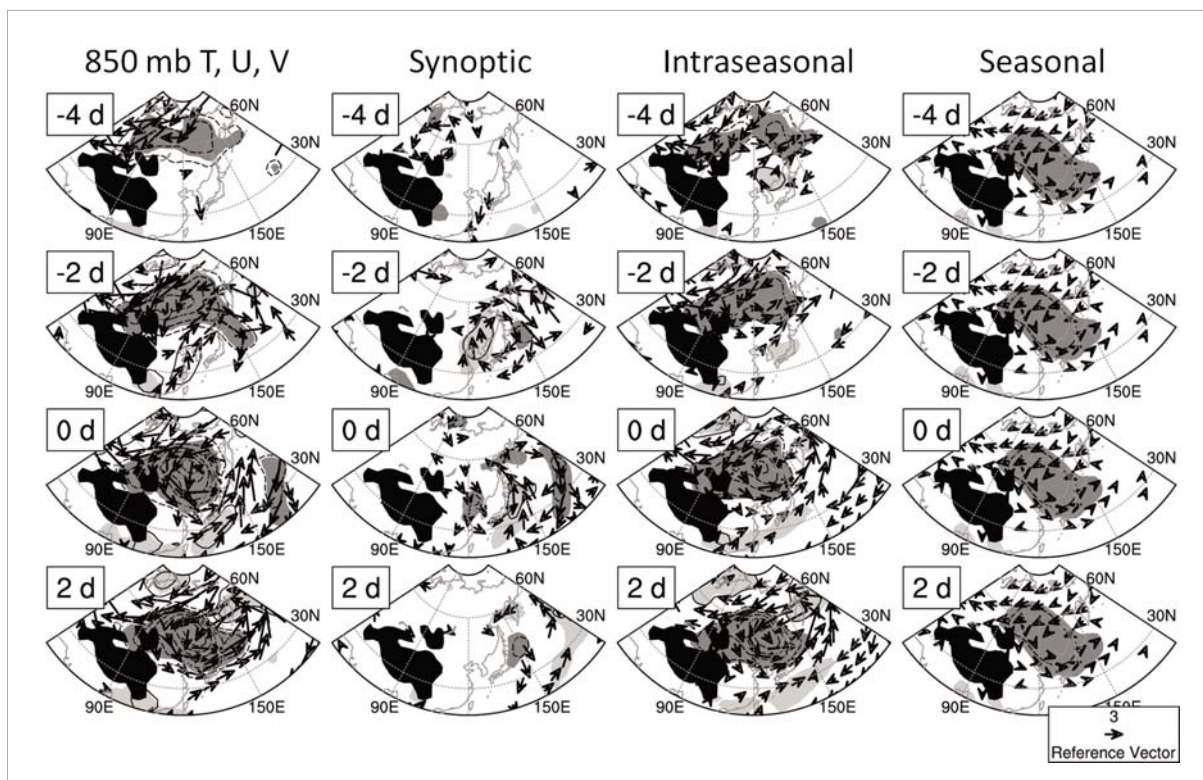


Figure 3. The modulations of the intraseasonal variation of the East Asian trough strength on the horizontal wind (vector; unit: m s^{-1}) and temperature at 850 hPa (contour; unit: m) (first column), from 4 days before to 2 days after the development of the intraseasonal strong East Asian trough. The modulations are also separated into synoptic (second column), intraseasonal (third column), and seasonal (fourth column) variations. The light (dark) shading signifies the positive (negative) temperature anomalies exceeding the 5% significance level.

References:

Leung, M. Y. T. and W. Zhou, 2015a: Vertical structure, physical properties and energy exchange of the East Asian trough in boreal winter. *Climate Dynamics*, 45, 1635–1656, doi: 10.1007/s00382-014-2419-7.

Leung, M. Y. T. and W. Zhou, 2015b: Variation of circulation and East Asian climate associated with anomalous strength and displacement of the East Asian trough. *Climate Dynamics*, doi: 10.1007/s00382-015-2504-6.

A3. Winter moisture supply over Southwest China

(PI: Wen ZHOU)

In this study, the anomalous moisture circulation associated with the interannual variation of the India-Burma Trough was investigated to examine how the trough affects the moisture supply to Southwest China in winter. It is noteworthy that the abnormal moisture convergence corresponding to the strong India-Burma Trough is constrained in a thin layer along the windward side of the Tibetan Plateau, with abnormal moisture divergence on top. It is the wind rather than moisture disturbance that dominates the total abnormal moisture convergence, with the former showing a similar pattern to that of the total abnormal moisture convergence (Figure 4). For more details, please refer to Li and Zhou (2016).

This study investigates how the India-Burma Trough modulates the interannual variation of the winter moisture supply over Southwest China.

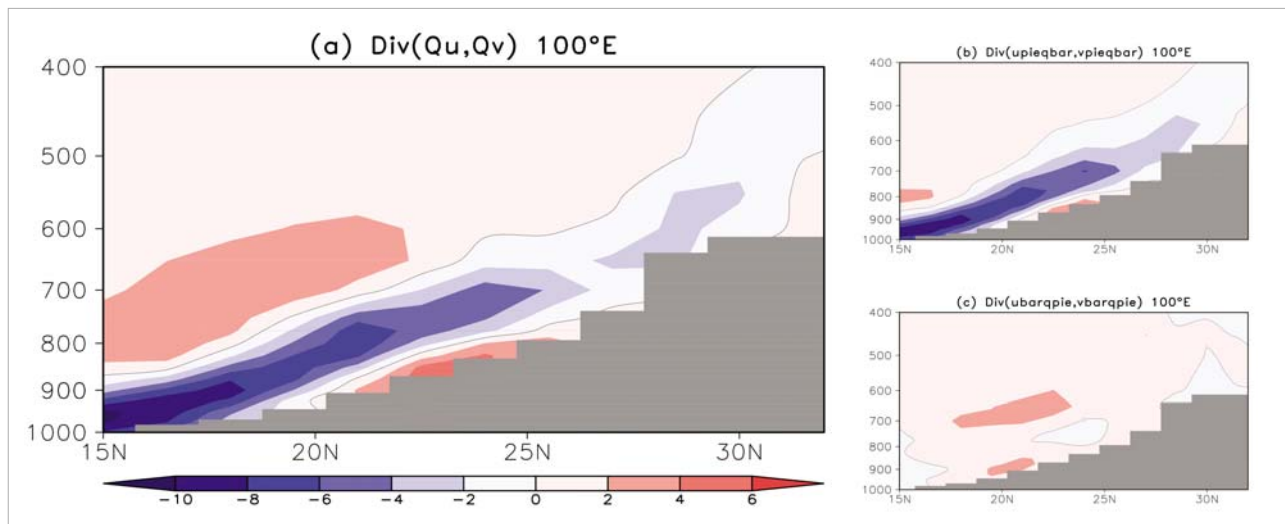


Figure 4. Vertical-meridional cross sections of moisture divergence along 100°E: (a) divergence of climatological moisture transported by abnormal wind, (b) divergence of abnormal moisture transported by climatological wind, and (c) divergence of abnormal moisture transported by abnormal wind. Unit is 10^{-9} s^{-1} .

Reference:

Li, X. Z. and W. Zhou, 2016: Modulation of the interannual variation of the India-Burma trough on the winter moisture supply over Southwest China. *Climate Dynamics*, 46, 147–158, doi: 10.1007/s00382-015-2575-4.

A4. Urban heat islands in Hong Kong: Statistical modeling and trend detection

(PI: Wen ZHOU)

Urban heat islands (UHIs), usually defined as temperature differences between urban areas and their surrounding rural areas, are one of the most significant anthropogenic modifications to the Earth's climate. The frequency of extreme UHI events in summer in Hong Kong is increasing significantly, which implies that the risk of mortality and heat-related diseases due to heat stress at night (when the daily maximum UHI occurs) is also increasing. The warming climate has threatened and will continue to threaten inhabitants of this subtropical high-density city. Strategies for adaptation to and mitigation of climate change, such as adding greenery and planning a city with good natural ventilation, are needed (Figure 5). For more details, please refer to Wang et al. (2015).

Extreme urban heat island events in summer in Hong Kong is increasing significantly. A frequency of one or two events per summer happens most often, while the maximum occurrence can be up to seven in one summer.

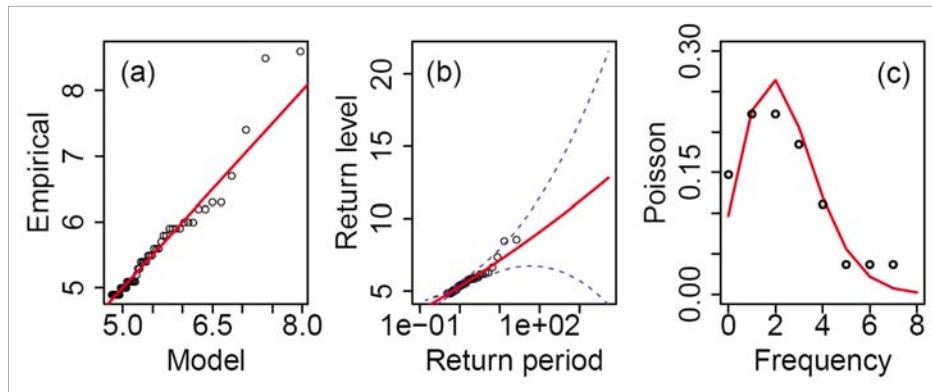


Figure 5. (a) Quantile plot, and (b) return level plot for GP distribution fitted to daily maximum UHI intensities in Hong Kong summers. (c) Frequency of extreme UHI events in Hong Kong summers fitted to the Poisson distribution. The threshold is 4.8°C.

Reference:

Wang, W. W., W. Zhou and E. Y. Y. Ng, 2015: Urban heat islands in Hong Kong: Statistical modeling and trend detection. Submitted to *Natural Hazards*. (under review)

A5. Multi-purpose rainwater harvesting for water resource recovery and the cooling effect (PI: Nicky LAM)

This study investigates the potential application of rainwater harvesting for water resources and urban heat island cooling to mitigate the impacts of climate change in Hong Kong.

A computational fluid dynamics model, ENVI-met, was employed to study the potential use of a rooftop for gardening and rainwater harvesting to reduce the urban heat island impacts in Hong Kong. A rainwater harvesting system not only provides a heat insulation layer for the rooftop, but also serves as reclaimed water storage for toilet flushing, which substantially reduces portable water usage in rural areas of Hong Kong where seawater flushing is not available. The noticeable temperature reduction is recorded as much as 1.3°C. Further comparison of system efficiency on the rainwater harvesting was performed between Hong Kong and Tokyo, Japan to study how the precipitation pattern may influence the effectiveness of the system (Figure 6).

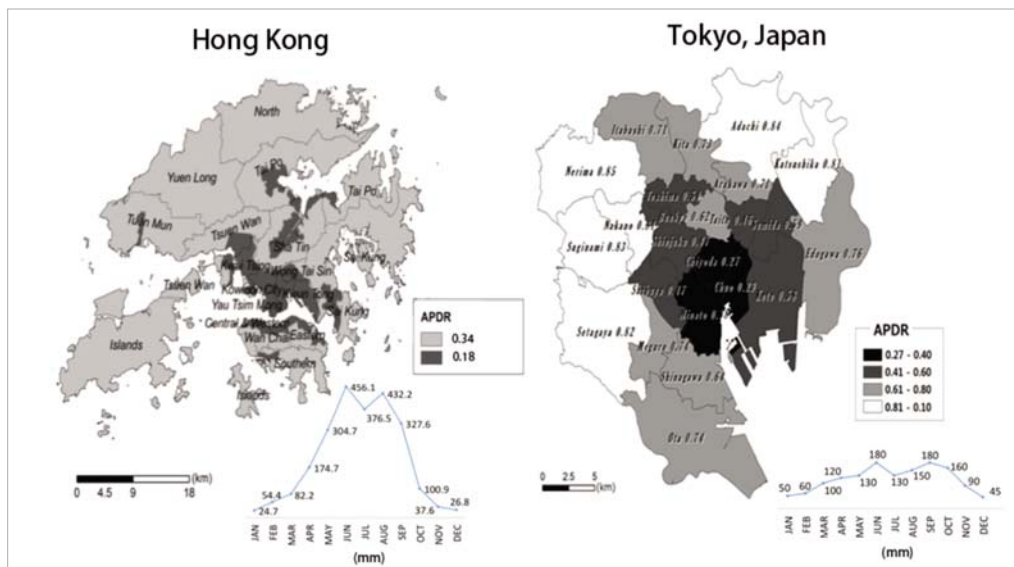


Figure 6. Area precipitation-demand ratio in sweater and fresh water flushing region in Hong Kong and Japan.

Reference:

An, K. J., Y. F. Lam, S. Hao, T. E. Morakinyo and H. Furumai, 2015: Multi-purpose rainwater harvesting for water resource and the cooling effect. *Water Research*, 86, 116–121, doi: 10.1016/j.watres.2015.07.040.

A6. Effect of sea surface temperature on local air temperature under high-resolution urban-canopy WRF in Hong Kong

(PI: Nicky LAM)

An urban-canopy weather research forecasting model (WRF-urban) was applied to study the effect of sea-surface temperature (SST) in high-resolution simulation for Hong Kong. Although the previous studies have stated the impacts of SST to local forecasting should be minimal, we have found that the impacts could be very large when it is under fine resolution simulation in the coastal areas in winter. Incorrectly prescribing SST (5°C difference between observation and NCEP global input) could result a 1-2°C differences in surface temperature prediction under WRF, while it intensifies when simulating under WRF-urban, as shown in Figure 7. Moreover, as demonstrated in the figure, accurately prescribing SST (FNL-33N-SSTOBS-UCM) would result in the best overall performance on surface temperature prediction, indicating that sea surface update on a daily basis using location observation is needed in fine-resolution weather forecasting in winter.

This study investigates the impacts of sea surface temperature in high-resolution urban-canopy WRF and its implications on local air quality forecasts.

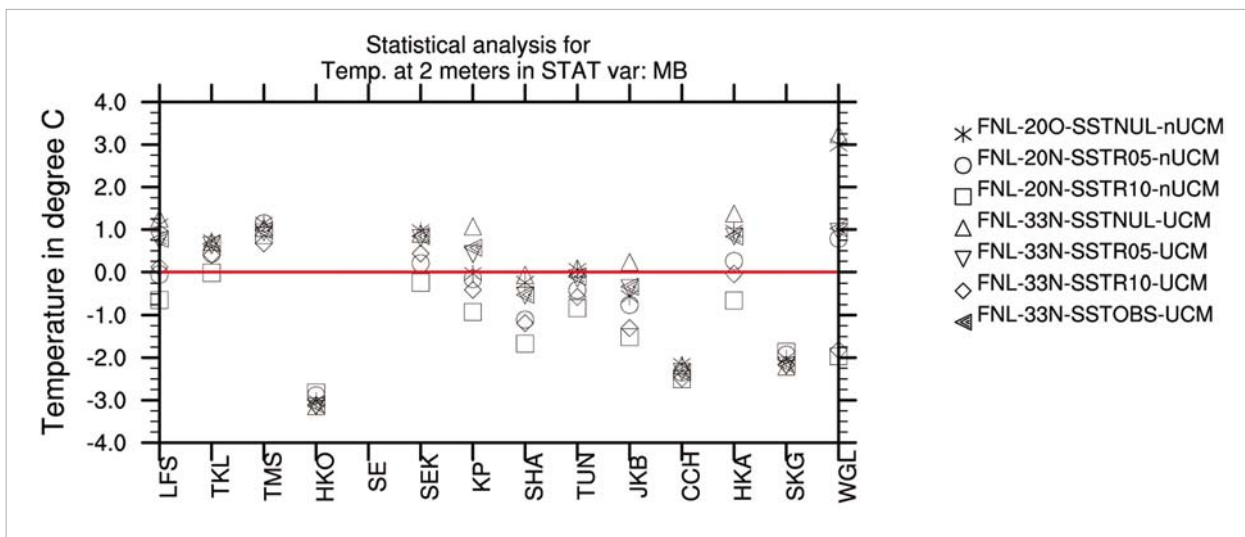


Figure 7. Statistical analysis (Mean Bias) for temperature at 2 m (nUCM means WRF; and UCM means WRF-urban).

B. Tropical Cyclone

B1. Decadal change of tropical cyclone landfall latitude along the East Asia coast

(PI: Johnny CHAN)

This study examines the decadal change of the mean tropical cyclone (TC) landfall latitude along the East Asian coast (from Vietnam to Japan) and a significant northward shift is identified in 1997 (Figure 8), suggesting a higher percentage of TCs making landfall in the regions north of Fujian, which is consistent with the upward trends of annual power dissipation index (APDI) in Zhejiang and the Korean Peninsula and the downward trend of APDI in Guangdong (Liu and Chan 2016).

This study identifies a northward shift in the mean tropical cyclone landfall latitude along the East Asian coast in the period 1997-2013.

The second EOF mode of the anomalous frequency of TC occurrence pattern, which represents the west-northwestward straight track across the Philippines and the South China Sea (SCS) and the northwestward straight track toward the east coast of China (Figure 9a), is generally in its negative phase during 1997-2007 (Figure 9b), suggesting a lower frequency of TCs making landfall in the south coast of China and Vietnam but a higher frequency for the east coast of China. The third EOF mode of the anomalous percentage of genesis frequency pattern, which represents the north-south shift in TC genesis location (Figure 9c), shows a significant shift in 1999 (Figure 9d), representing a northward shift in genesis location during 1999-2013. On the other hand, a large area of negative anomalies extending from the northern part of the SCS to the ocean east of Japan is found during 1997-2013 (Figure 10a), indicating weaker vertical wind shear in these areas, which allows the TCs approaching the coastal areas to intensify and gain higher intensity before landfall. Indeed, the time series of the mean vertical wind shear in the region 15°-30°N, 120°-150°E clearly shows a downward shift in 2000 (Figure 10b), which suggests a favorable atmospheric environment for TC intensification and more TCs with higher intensity near the coastal areas since then. All of these factors lead to more intense TCs making landfall in the northern part of East Asia and therefore a greater threat of strong TC landfalls is found in the regions including Zhejiang, the Korean Peninsula and Japan.

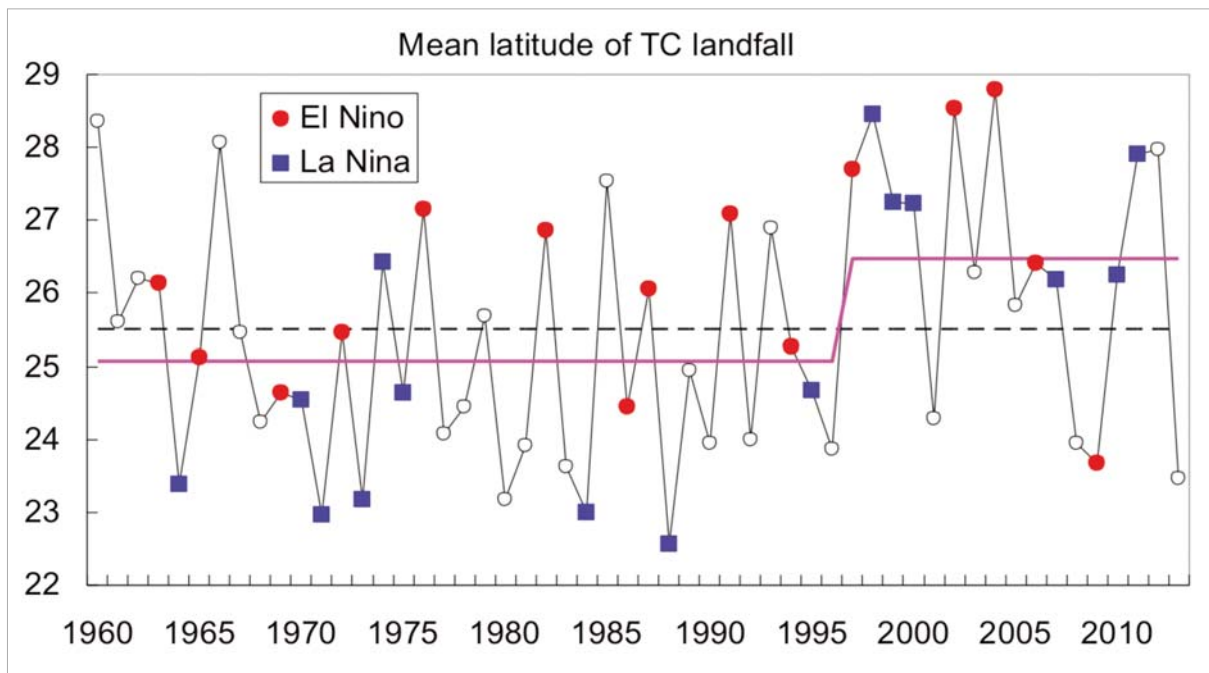


Figure 8. Time series of the mean latitude of TCs making landfall along the East Asian coast in the months from June to October during the period 1960-2013. Solid circles and squares indicate El Niño and La Niña years respectively. The horizontal dashed line indicates the climatological mean and the solid lines indicate the possible regime shifts.

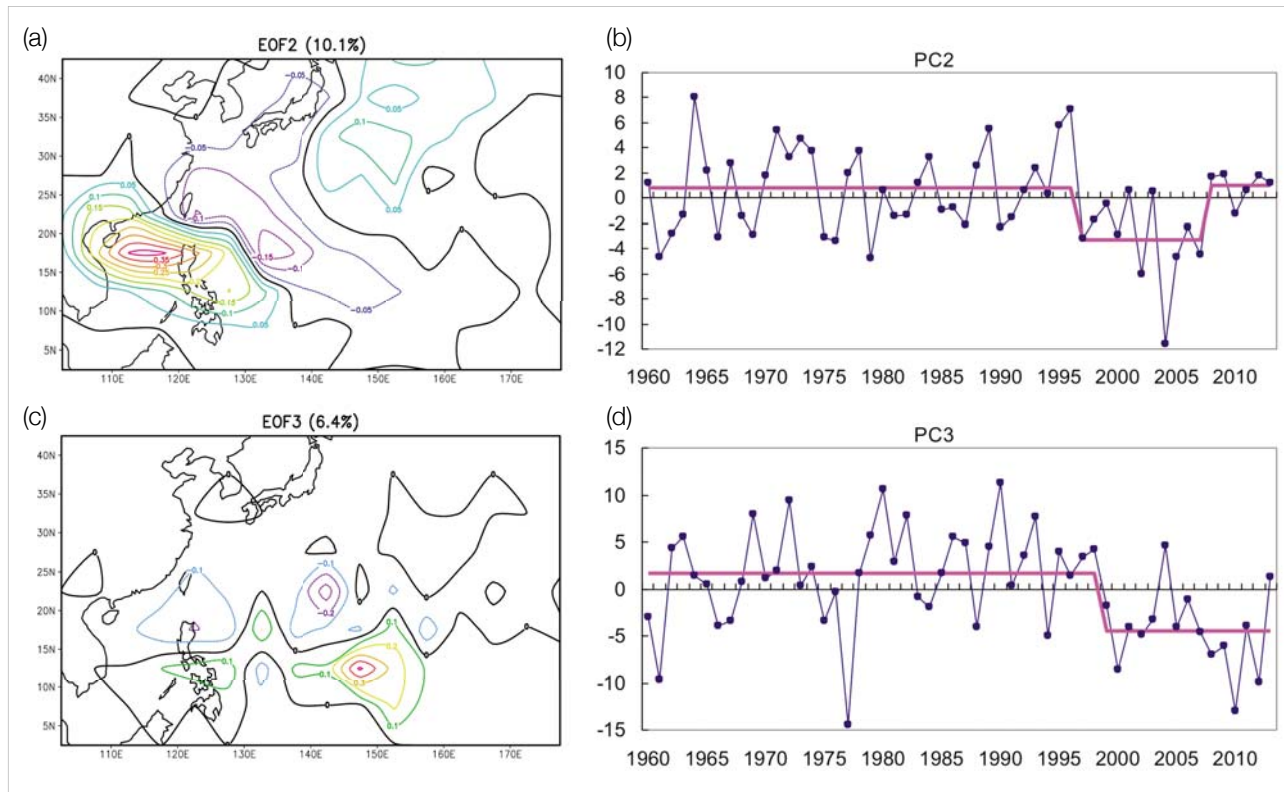


Figure 9. (a) Loading patterns of the TC occurrence pattern for the second mode and (b) the time series of the PC2 coefficient. (c) Loading pattern of anomalous percentage of genesis frequency for the third mode and (d) the time series of the PC3 coefficients. The horizontal lines indicate the possible regime shifts.

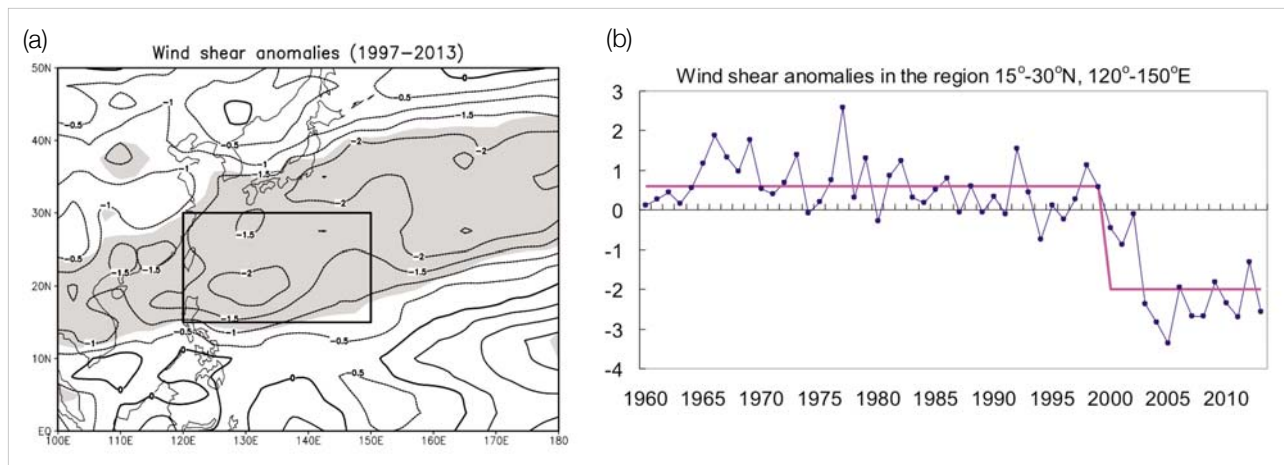


Figure 10. (a) Pattern of Jun-Oct vertical zonal wind shear anomalies in the period 1997-2013. Shadings indicate the anomalies are significant at the 95% confidence level. (b) Time series of the average vertical wind shear anomalies in the region 15° - 30° N, 120° - 150° E as shown in the rectangular box in (a).

Reference:

Liu, K. S. and J. C. L. Chan, 2016: Variations in the power dissipation index in the East Asia region. *Climate Dynamics*, doi: 10.1007/s00382-016-3185-5.

B2. Summary of 2015 seasonal forecasts of tropical cyclone activity in East Asia

(PI: Judy HUANG and Johnny CHAN)

Based on the dynamical downscaling procedure developed by Huang and Chan (2014), this study evaluates the ability of a regional climate model (RegCM3) driven by CFSv2 real time forecast data to predict 2015 seasonal tropical cyclone (TC) activity. The evaluations focus on the forecasts of TC genesis over the western North Pacific (WNP) region (Figure 11a), and the forecasts of TCs making landfall in various parts of East Asia (Figures 11b-d). The forecasts began in March 2015 and the model was run at the beginning of each month with eight ensemble members until September 2015. In 2015, the observation (JTWC) shows that the number of WNP-TC genesis as well as the number of TCs making landfall in the MTC region (covering Taiwan, Fujian, Zhejiang and Jiangsu provinces, and Shanghai municipality) and in the STC region (covering South China, Vietnam and the Philippines) are all below the climatology (estimated from the mean of TCs during 2000-2010). In contrast, the number of TCs making landfall in the NTC region (covering Korean peninsula and Japan) are close to the climatology (within ± 1). By comparing these observational features to those predicted by RegCM3 and CFSv2, this study finds that RegCM3 performs better than CFSv2 in predicting the number of WNP-TC genesis. The close forecast (within ± 1) from RegCM3 is the one initiated in May (for JJASON), June (for JASOND) and August (for SOND). Regarding to TCs making landfall in various parts of East Asia, the overall forecast skill from RegCM3 is also higher than that from CFSv2, particularly for the one initiated in April (for MJJASO) and May (JJASON), and for the MTC and STC regions. As for the NTC region, the close forecast (within ± 1) from RegCM3 is the one initiated in June (for JASOND) and August (for SOND). A summary of these forecasts is given in Figure 11. Other details can be found in http://www.cityu.edu.hk/gcacic/Research_Brief_201501.pdf.

This study examines the dynamical downscaling prediction of tropical cyclone activity in East Asia for 2015 April to December. Results show that the forecast skill from the dynamical downscaling procedure (i.e. RegCM3) is generally higher than that from CFSv2.

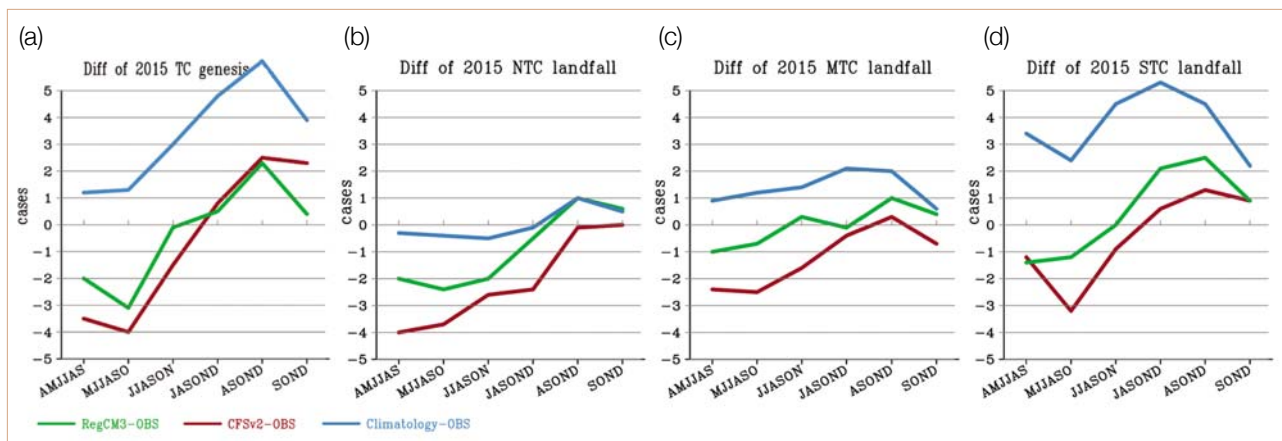


Figure 11. (a) Summary of TC genesis over the western North Pacific region in 2015. (b) to (d), Summary of TCs making landfall over various parts of East Asia (NTC – north TCs: those making landfall in the Korean Peninsula and Japan, MTC – middle TCs: those making landfall in Taiwan, Fujian, Zhejiang and Jiangsu provinces, and Shanghai municipality, and STC – south TCs: those making landfall in South China, Vietnam and the Philippines). The green lines are the differences between forecasts from RegCM3 and observation from JTWC. The red lines are the differences between forecasts from CFSv2 and observation from JTWC. The blue lines are the differences between climatology (mean of 2000-2010) and observation from JTWC.

Reference:

Huang, W. R. and J. C. L. Chan, 2014: Dynamical downscaling forecasts of western North Pacific tropical cyclone genesis and landfall. *Climate Dynamics*, 42, 2227–2237.

B3. Change in destructiveness of landfalling tropical cyclones over China

(PI: Wen ZHOU)

This study investigates changes in the destructiveness of landfalling tropical cyclones (TCs) over China during 1975–2014. Diagnostic analysis suggests that the reduction in TC occurrence over South China offsets considerably the positive effects of the intensity and the nonlinear term. The southeasterly flows on the eastern flank of the cyclonic circulation tend to favor subsequent landfall of TCs over East China (TC_{EC}), resulting in an increase in landfall frequency, which contributes in part to the enhanced power dissipation index (PDI) of TCs over this region. Meanwhile, the slowing down of the mean translation speed of TC_{EC} and the weakening of vertical wind shear tend to favor the intensification of TC_{EC} , leading to an increase in intensity and hence the PDI of TCs over East China (Figure 12). For more details, please refer to Li and Zhou (2015).

It is found that tropical cyclones making landfall over East China have tended to be more destructive in recent decades, with a significant increase in the power dissipation index after landfall.

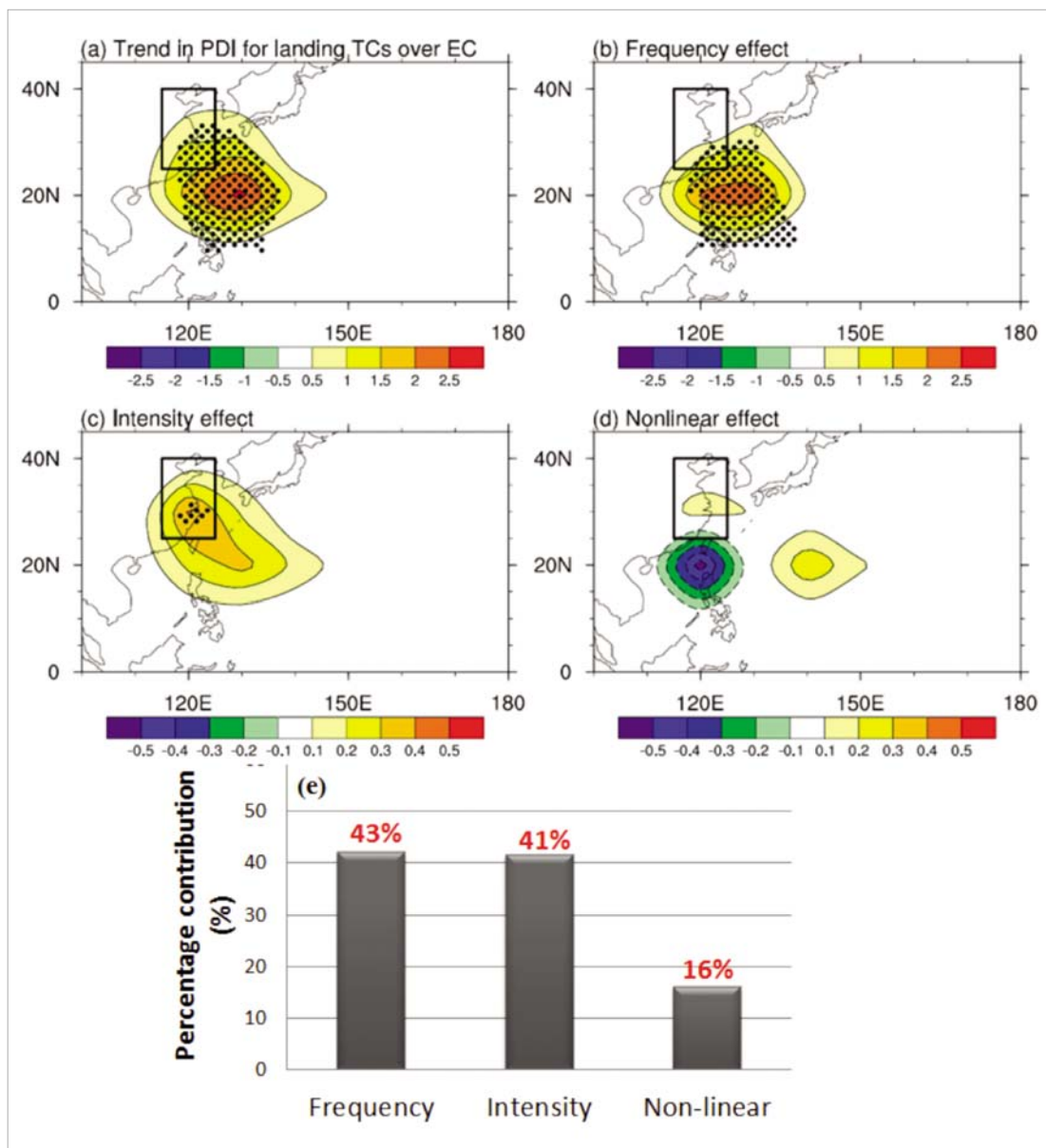


Figure 12. Linear trends of (a) PDI ($10^5 \text{ kt}^3/\text{decade}$) for TC_{EC} and the contribution of the (b) frequency effect, (c) intensity effect, and (d) nonlinear effect to the PDI trend during 1975–2014. Regions with trends that are significant at 90% confidence level are shaded by dots. The associated percentage contributions of each of the terms to the overall trend in PDI over EC (as indicated by the rectangles) are shown in (e).

Reference:

Li, C. Y. and W. Zhou, 2015: Change in destructiveness of landfalling tropical cyclones over China in recent decades. Submitted to Journal of Climate. (Under review)

C. Air Quality

C1. Speciation of water soluble iron with a novel dispersive absorption spectroscopic measurement technique

(PI: Zhi NING)

A very low detection limit spectroscopic measurement method for iron speciation was developed.

In this study, we developed and evaluated a dispersive absorption spectroscopic technique for trace level soluble ferrous detection. The state of iron in aerosols is considered an important factor in toxicity and atmospheric chemistry. The technique makes use of the broadband absorption spectra of the ferrous-ferrozine complex with a novel spectral fitting algorithm to determine soluble ferrous concentrations in samples and achieves much improved measurement precision compared to conventional methods. The developed method was evaluated by both model simulations and experimental investigations. Figure 13 shows a schematic of the experimental system. A PC is connected to the spectrometer to log and process the data. Study results demonstrated the robustness of the method against spectral fluctuation, wavelength drift and electronic noise, while achieving excellent linearity ($R^2 > 0.999$) and low detection limit ($0.06 \mu\text{g L}^{-1}$) for soluble ferrous detection. The developed method was also used for the speciation of soluble iron from size segregated atmospheric aerosols. Measurements were carried out during spring and summer of 2015 in typical urban environment in Hong Kong. The measured total iron concentrations are in good agreement with conventional, but costly Inductively Coupled Plasma - Optical Emission Spectroscopy (ICP-OES) measurements as can be seen in Figure 14. When this system was employed in investigations of ambient particulate matter samples, we established the size dependent characteristic of iron speciation in the atmosphere. Fine particles were found to play a more active role in transforming between ferrous and ferric than larger particles. The method demonstrated in this study provides a cost and time effective approach for the speciation of iron in ambient aerosols. The time dependence of analytic procedures and the role of water quality is shown in Figure 15.

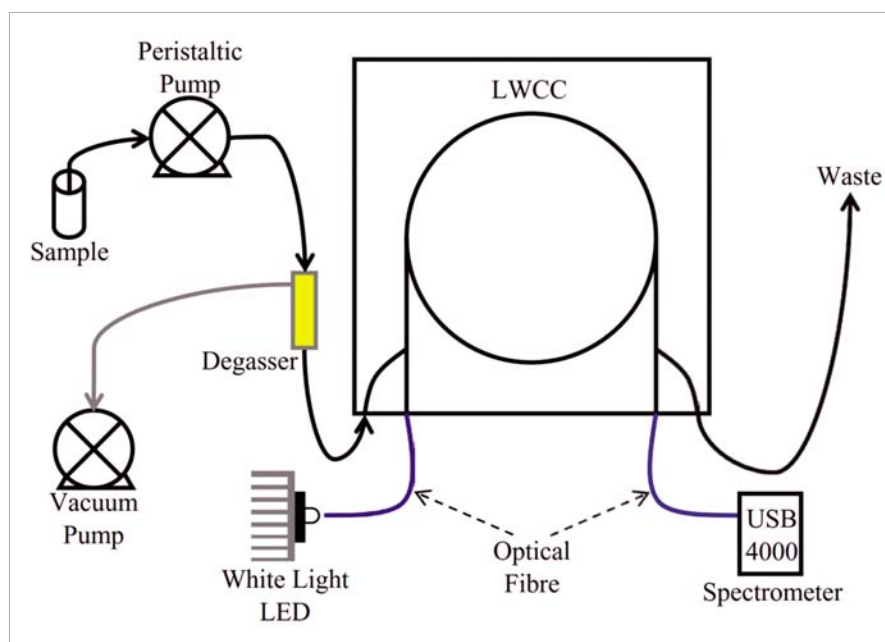


Figure 13. Schematic diagram of the experimental setup of the LED-based liquid waveguide capillary cell (LWCC) for optical absorption detection of water soluble Fe(II).

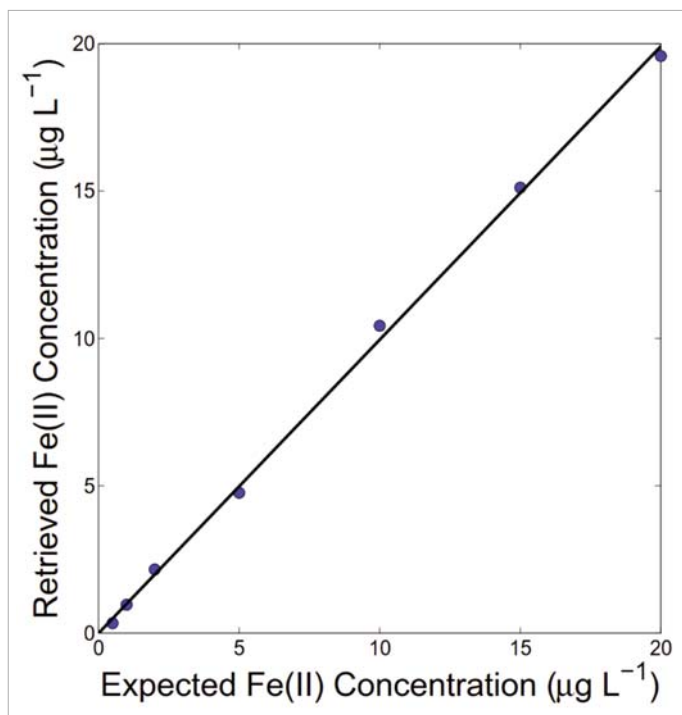


Figure 14. Validation of the dispersive absorption measurement of Fe(II). X-axis shows the Fe(II) concentration of the standard solutions. Y-axis shows the retrieved Fe(II) concentrations using the dispersive absorption spectroscopy with the fitting algorithm.

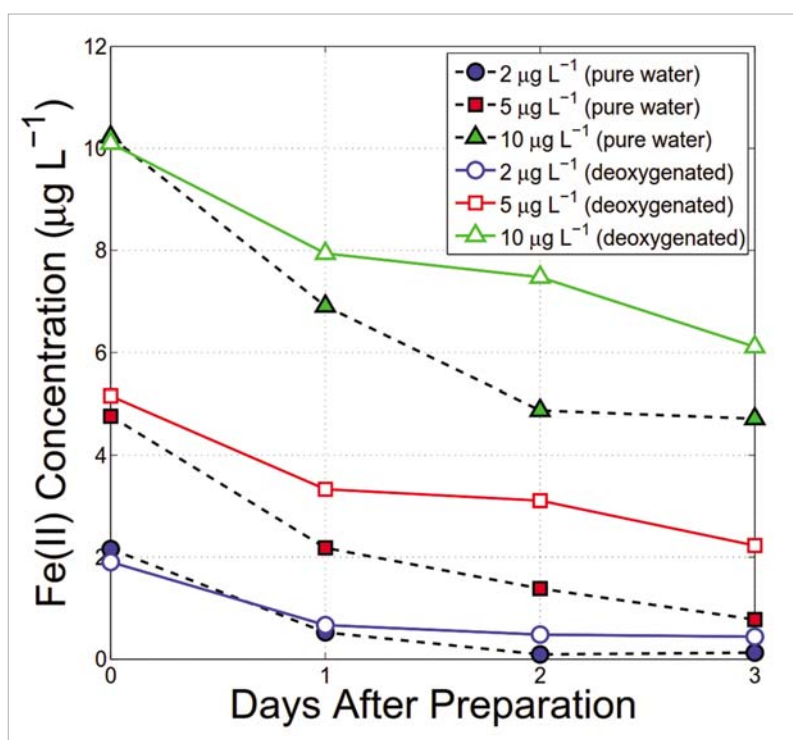


Figure 15. Decay trends of Fe(II) in the solutions. Standard solutions with Fe(II) concentration levels of 2 $\mu\text{g L}^{-1}$, 5 $\mu\text{g L}^{-1}$ and 10 $\mu\text{g L}^{-1}$ were analyzed. The solutions were analyzed immediately, 1 day, 2 days and 3 days after preparation to investigate the stability of Fe(II) in the solution. Both pure water (dotted line) and deoxygenated water (solid line) were used for the preparation of standard solutions.

Reference:

Chan, K. L., S. Y. N. Jiang and Z. Ning, 2016: Speciation of water soluble iron in size segregated airborne particulate matter using LED based liquid waveguide with a novel dispersive absorption spectroscopic measurement technique. *Analytica Chimica Acta*, 914, 100–109.

C2. Development and application of a next generation air sensor network

(PI: Zhi NING)

This study focused on the development and evaluation of a next generation air monitoring system with both laboratory and field tests. The system was developed to allow flexible air monitoring at sites where existing routine air monitoring programs are not adequate to estimate pollution conditions. A schematic of the monitor system is shown in Figure 16. It consisted of a size selective inlet that was followed by a photometer unit (ES-642, MetOne, USA) that reported PM 2.5 mass. Two gas sensors; one for nitrogen dioxide (NO₂) and the other for carbon monoxide (CO) sensed these gases. The system was linked to a custom built electronics package and was powered by a rechargeable battery. A multi parameter algorithm was used to process the voltage-based signal from each sensor to correct for the impact of environmental conditions on the electrochemical sensors for CO and NO₂. Ozone was measured by a separate monitor, the POM (Personal Ozone Monitor, 2be Technology, USA). Table 1 presents the overall characteristics of the air sensor system. Multiple sets of the developed system were then deployed in the Hong Kong Marathon 2015 forming a sensor based network along the Marathon route as illustrated in Figure 17. Real time air pollution concentration data were wirelessly transmitted and the Air Quality Health Index (AQHI) for the Green Marathon was calculated, which were broadcast to the public on hourly basis. The route-specific sensor network showed somewhat different pollutant patterns than routine air monitoring, indicating the immediate impact of traffic control during the Marathon on the roadside air quality. Field evaluation of the sensor performance are shown in Figures 18-20 in an urban roadside environment in comparison to government operated reference monitors showed good agreement with measurement error within 5% of the pollutant concentrations. The study is one of the first applications of next generation sensor network in international sport events and it demonstrated the usefulness of the emerging sensor based air monitoring technology in rapid network deployment to supplement existing air monitoring.

We have developed the first-ever international sport event based air sensor network for public communication.

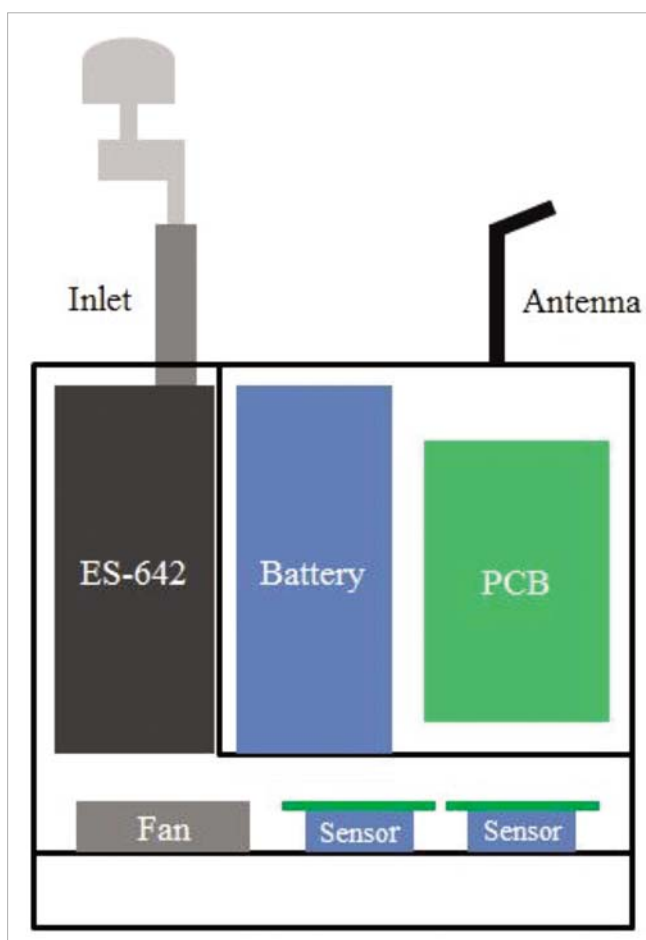


Figure 16. Schematic of Mini Air Station (MAS) system with different components.

Table 1. Specifications of NO₂ and CO sensors, ES-642 and POM.

Pollutant	Sensor	Sensitivity	Response Time	Measurement Range	Zero Drift
NO ₂	NO ₂ -B4	-250 to -600nA/ppm at 2 ppm NO ₂	<25s from zero to 10ppm NO ₂	0-20ppm	0 to 20 ppb change/year in lab air
CO	CO-B4	420 to 650nA/ppm at 2 ppm CO	<15s from zero to 10ppm CO	0-1000ppm	<±100ppb change/year in lab air
PM _{2.5}	ES642-PM _{2.5}	0.001mg/m ³	NA	0 to 100mg/m ³	Automatic zero every hour
O ₃	POM	2ppb	20s for 100% of step change	2ppb to 10ppm	<2ppb/day

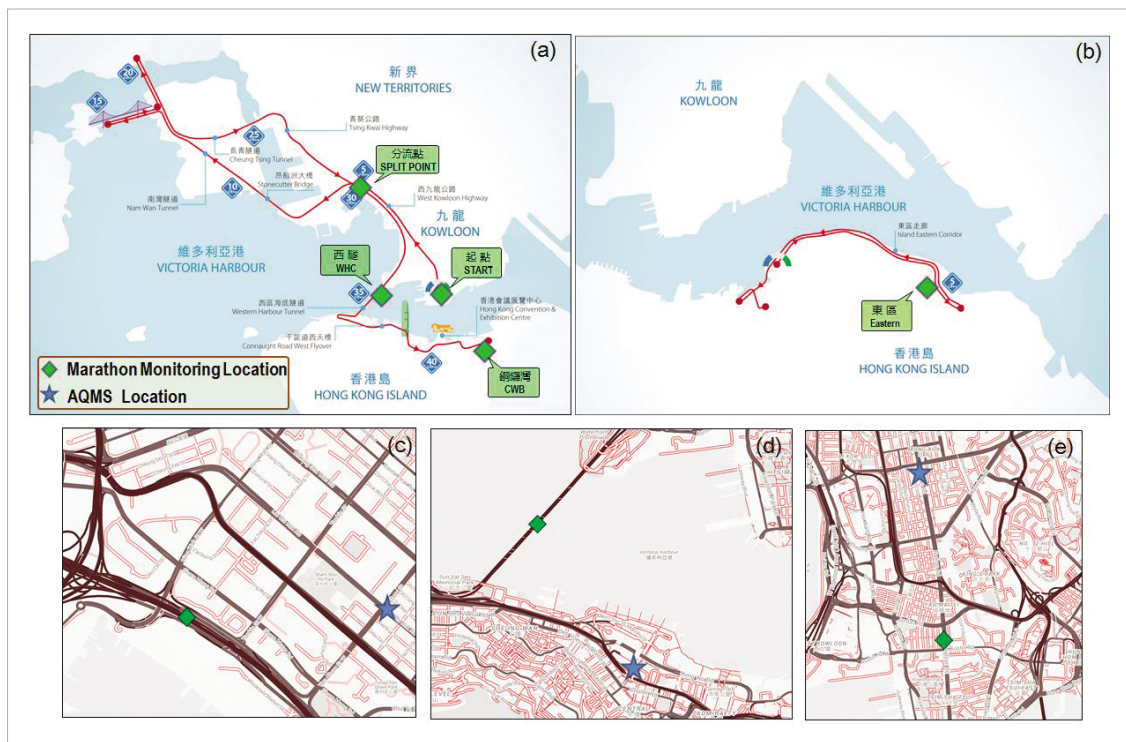


Figure 17. Air monitoring stations along (a) full/half marathon route; (b) 10km marathon route; and nearby AQMS run by HKEDP (c) Sham Shui Po AQMS near SSP; (d) Central AQMS near WHC;(e) Mong Kok AQMS near TST.

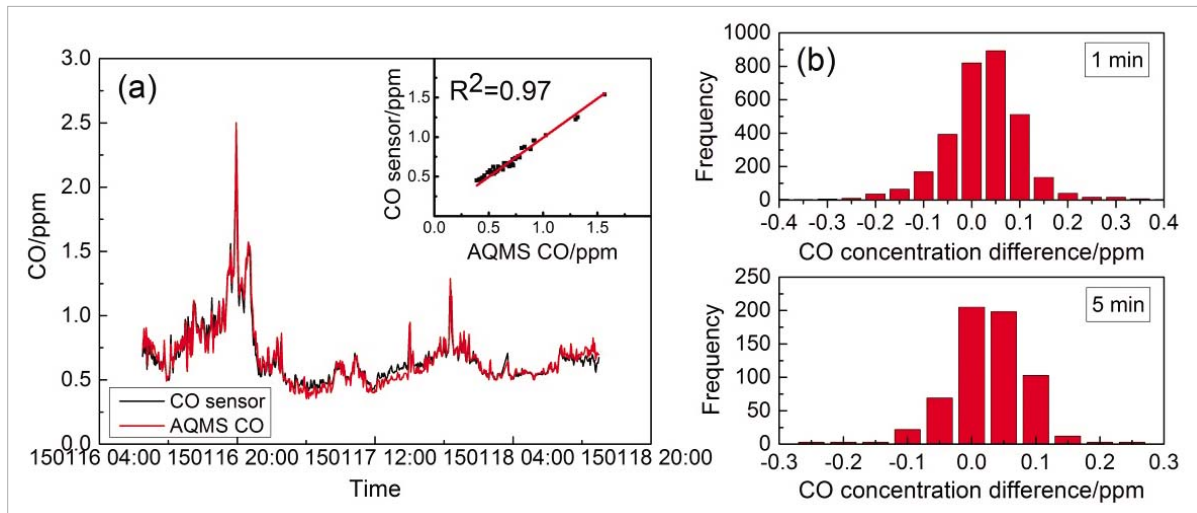


Figure 18. Comparison of the CO concentration from MAS and AQMS. (a) Time series of concentration; (b) Histogram of concentration difference in 1-min and 5-min time average.

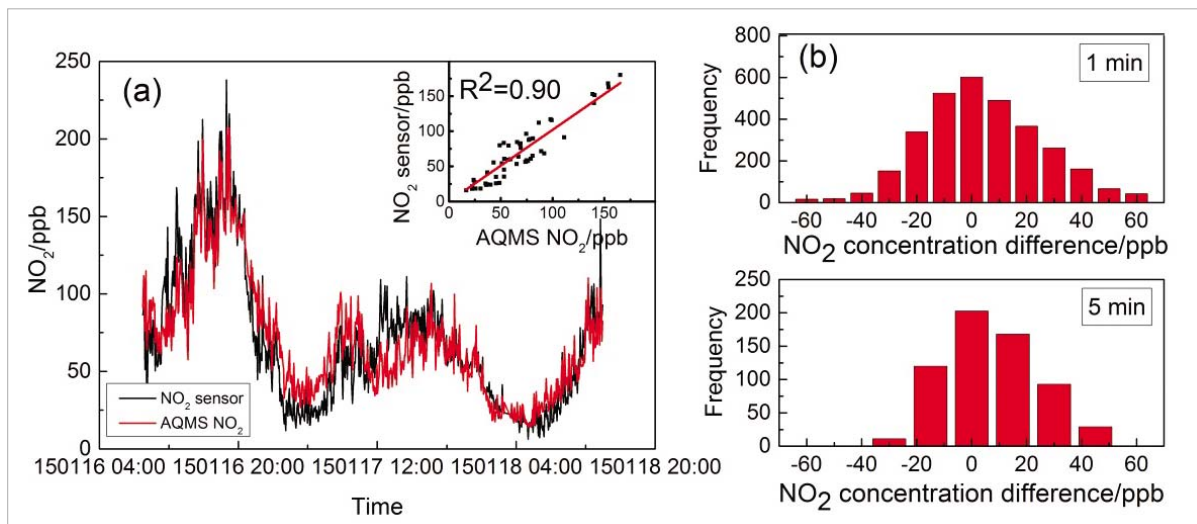


Figure 19. Comparison of the NO₂ concentration from MAS and AQMS. (a) Time series of concentration; (b) Histogram of concentration difference in 1-min and 5-min time average.

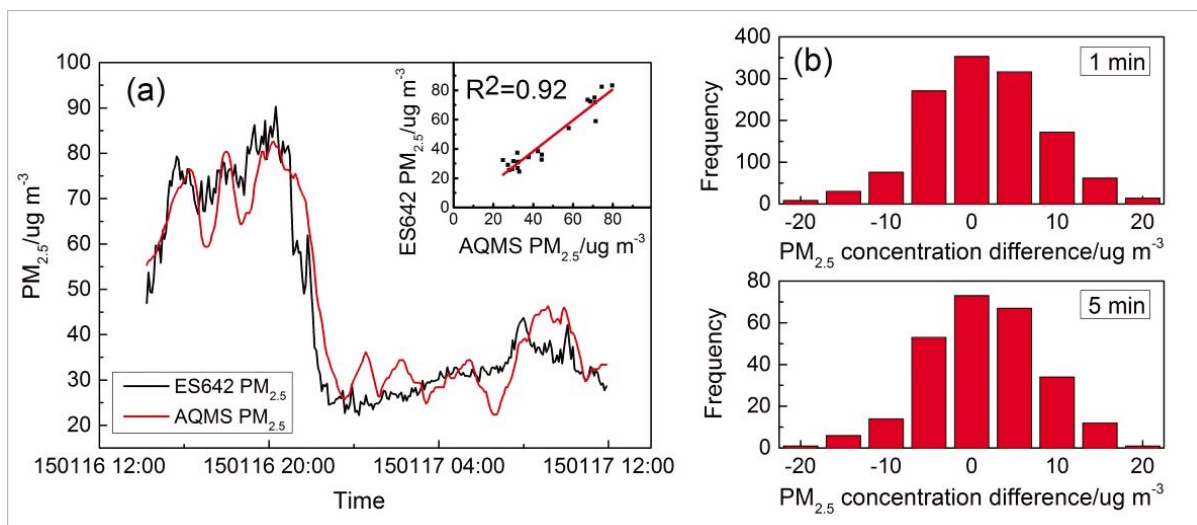


Figure 20. Comparison of the PM_{2.5} concentration from MAS and AQMS. (a) Time series of concentration; (b) Histogram of concentration difference in 1-min and 5-min time average.

Reference:

Sun, L., K. C. Wong, P. Wei, S. Ye, H. Huang, F. Yang, D. Westerdahl, P. K. K. Louie, C. W. Y. Luk and Z. Ning, 2016: Development and application of a next generation air sensor network for the Hong Kong marathon 2015 air quality monitoring. *Sensors (Switzerland)*, 16 (2), 18 p.

C3. Evaluation of diesel fleet emissions and control policies from plume chasing measurements of on-road vehicles

(PI: Zhi NING)

Vehicle emissions are an important source of urban air pollution. Diesel fuelled vehicles, although constituting a relatively small fraction of fleet population in many cities, are significant contributors to the emission inventory due to their often long mileage for goods and public transport. Further, until very recently the emissions from these vehicles have proven difficult to control. Recent classification of diesel exhaust as carcinogenic by the World Health Organization also raises attention to more stringent control of diesel emissions to protect public health. Although various mandatory and voluntary based emission control measures have been implemented in Hong Kong, there have been few investigations to evaluate if in-use fleet emission characteristics have met desired emission reduction objectives and if adoption of an Inspection/Maintenance (I/M) programme has been effective in achieving these objectives. The limitations are partially due to the lack of cost-effective approaches for the large scale characterization of fleet based emissions to assess the effectiveness of control measures and policy.

A comprehensive evaluation of the fleet-based diesel vehicle emissions in Hong Kong was carried out.

This study has used a plume chasing method to collect a large amount of on-road vehicle emission data of Hong Kong highways and a detailed analysis was carried out to provide a quantitative evaluation of the emission characteristics in terms of the role of high and super-emitters in total emission reduction, impact of after-treatment on the multi-pollutants reduction strategy and the trend of NO₂ emissions with newer emission standards. The plume chasing approach used in this study proves to be a cost-effective way of assessing city wide vehicle emission characteristics of actual vehicles in use on road. In summary, this method involves following vehicles of interest and measuring concentrations of pollutants such as oxides of nitrogen, carbon monoxide, particulate matter, black carbon as well as carbon dioxide. Observations of vehicle related changes in these pollutants are incorporated along with known factors that include fuel characteristics in calculations that produce vehicle specific emission factors (EF). Vehicle license numbers are also recorded which allows vehicles to be separated into “Euro” emission classes by vehicle types (such as franchised buses (FB) and Heavy duty trucks (HDV)). Data from the study are shown in Figure 21 for two pollutants that are especially of concern for diesel powered vehicles. Figure 22 shows the data in another view of the findings of the study. It shows NO_x emissions standards vs. the observed values from the actual on road chase findings. The FB values show data consistent with effective controls while HDV do not show full compliance with standards in older vehicles that continue into the most current Euro V vehicles. The second panel of Figure 22 illustrates a different pattern. Emissions of particulate matter have fallen as emission standards have tightened to Euro V for all vehicles tested. One possible explanation of the findings for NO_x is that the two types of vehicles may be receiving differing service or that NO_x controls are not as effective while on road when compared to test bed compliance testing.

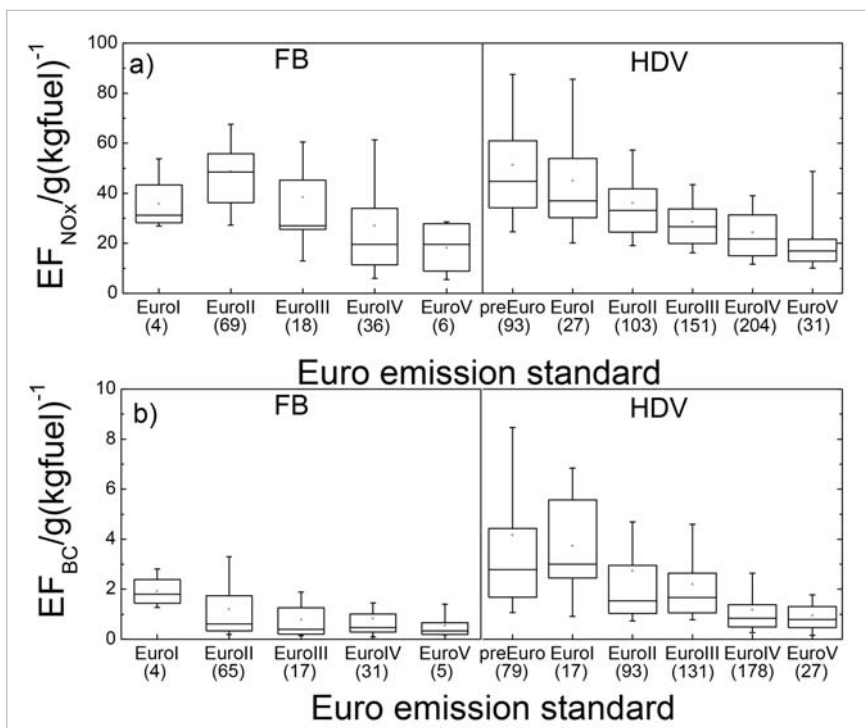


Figure 21. Boxplots of emissions from different fleets by vehicle design standards. a) NO_x ; b) BC. Numbers in the parentheses are vehicle counts by Euro class.

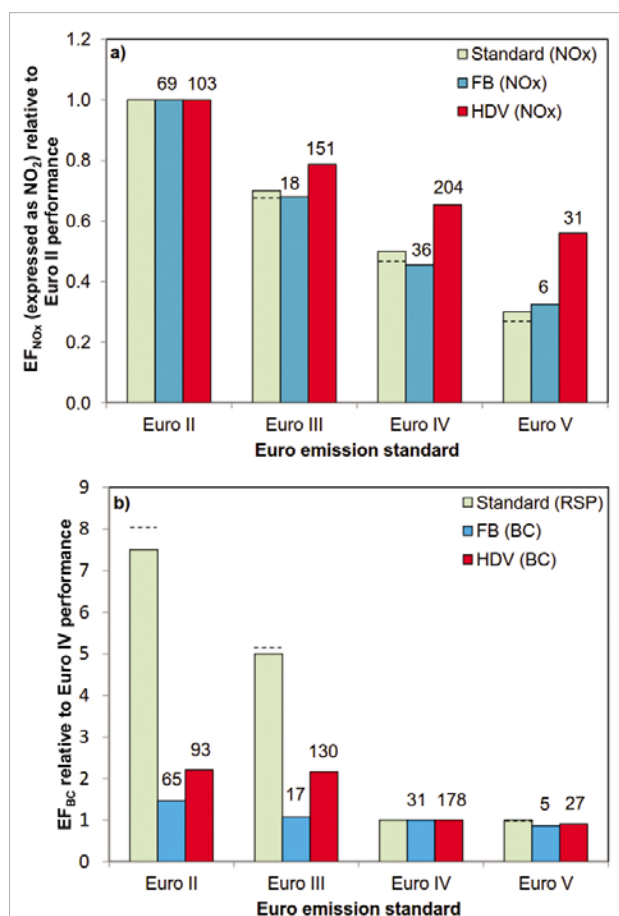


Figure 22. Comparison of the Euro standard with mean observed emission factors of different fleets (FB and HDV). a) NO_x emission factor b) BC emission factor with RSP surrogate for standard. The numbers on top of the bars are vehicle counts.

Reference:

Lau, C. F., A. Rakowska, T. Townsend, P. Brimblecombe, T. L. Chan, Y. S. Yam, G. Močnik and Z. Ning, 2015: Evaluation of diesel fleet emissions and control policies from plume chasing measurements of on-road vehicles. *Atmospheric Environment*, 122, 171–182, doi: 10.1016/j.atmosenv.2015.09.048.

C4. Top-down emission inventory development for fine resolution simulation

(PI: Nicky LAM)

Emission inventory developed using a top-down method has been widely used in the developing countries for estimating local emissions that are used for the photochemical grid modelling (CMAQ). The application of fine resolution (10 km or below) in the top-down method is often limited by insufficient information from the industrial sector/minor point sources. In China, the traditional way of using population density to allocate these industrial emissions has been found to be inaccurate/insufficient due to the change of urbanization pattern from “live nearby industry” to “live away from industry” for fine resolution modelling. In this study, a new method that is using image processing technique from Google map has been tested in the 3-km Shanghai domain. The results show that the “industrial allocation” significantly improves the spatial pattern of local emissions (Figure 23) and gives reasonable estimates for the minor point sources in the fine resolution CMAQ more than the traditional population-oriented allocation method. Although the method is lacking accurate information on the emission rates for individual sources, it has still been found to be a good method for use in fine resolution emission modelling in China.

This study describes a new satellite image processing method for reallocating industrial emissions in the development of top-down emission inventory for fine-resolution air quality and climate simulation in China.

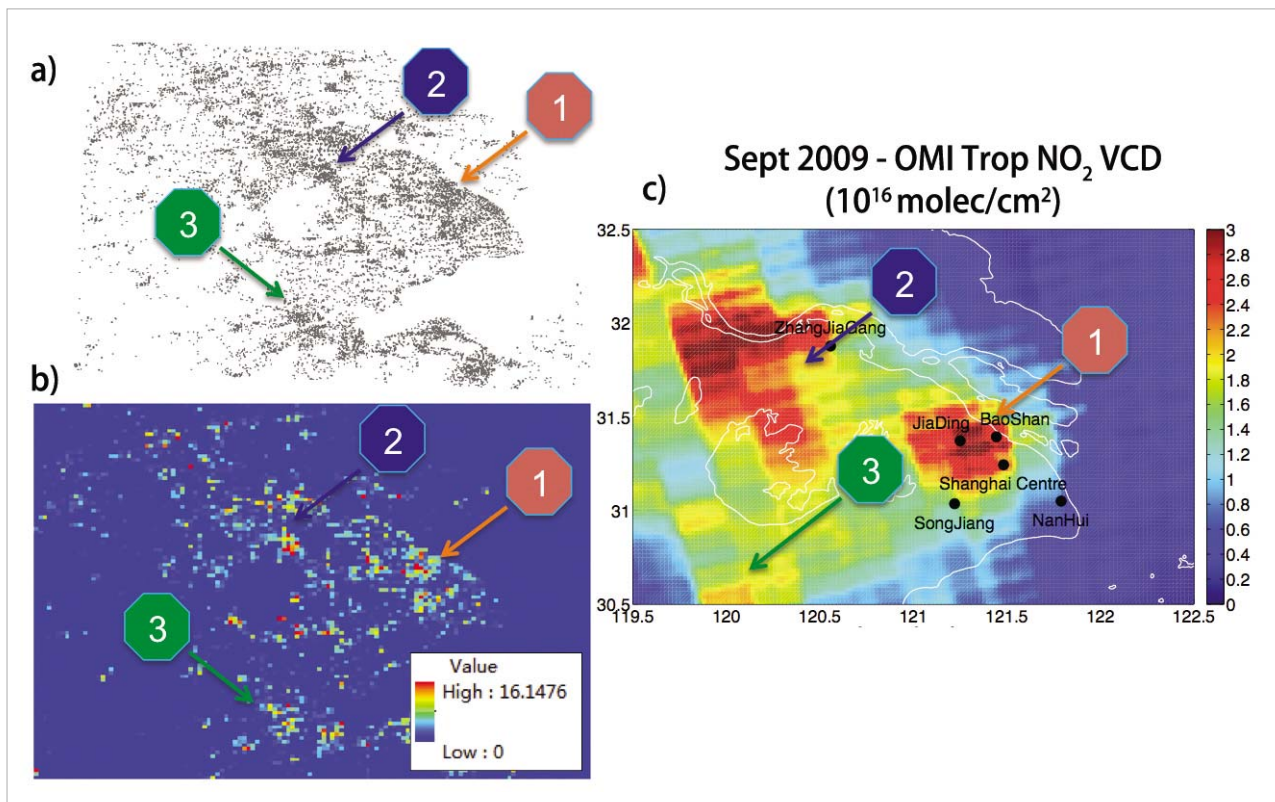


Figure 23. a) Spatial distribution of industrial emission; b) area percentage of industrial areas within 3-km resolution grid, and OMI tropospheric NO₂ vertical column density in September 2009.

C5. Synoptic weather control of summer air quality in Hong Kong

(PI: Wen ZHOU)

This study investigates the influence of atmospheric circulation on air pollution levels in Hong Kong in summer. Pollution roses of daily average surface air pollution monitoring data, with sounding wind data at different vertical levels, reveal a stronger relationship at an elevation of 1500 m than at 100 m above the surface, which may have an influence on the surface. Based on analysis of the HYSPLIT model, high pollution levels in summer are highly related to wind flow from the west, north, and northwest. The Western North Pacific Subtropical High (WNPSH) has a strong influence on air pollution levels in Hong Kong via wind and atmospheric stability (Figure 24). For more details, please refer to Chow et al. (2015).

Pollution roses of daily average surface air pollution monitoring data reveal a stronger relationship at an elevation of 1500 m than at 100 m above the surface.

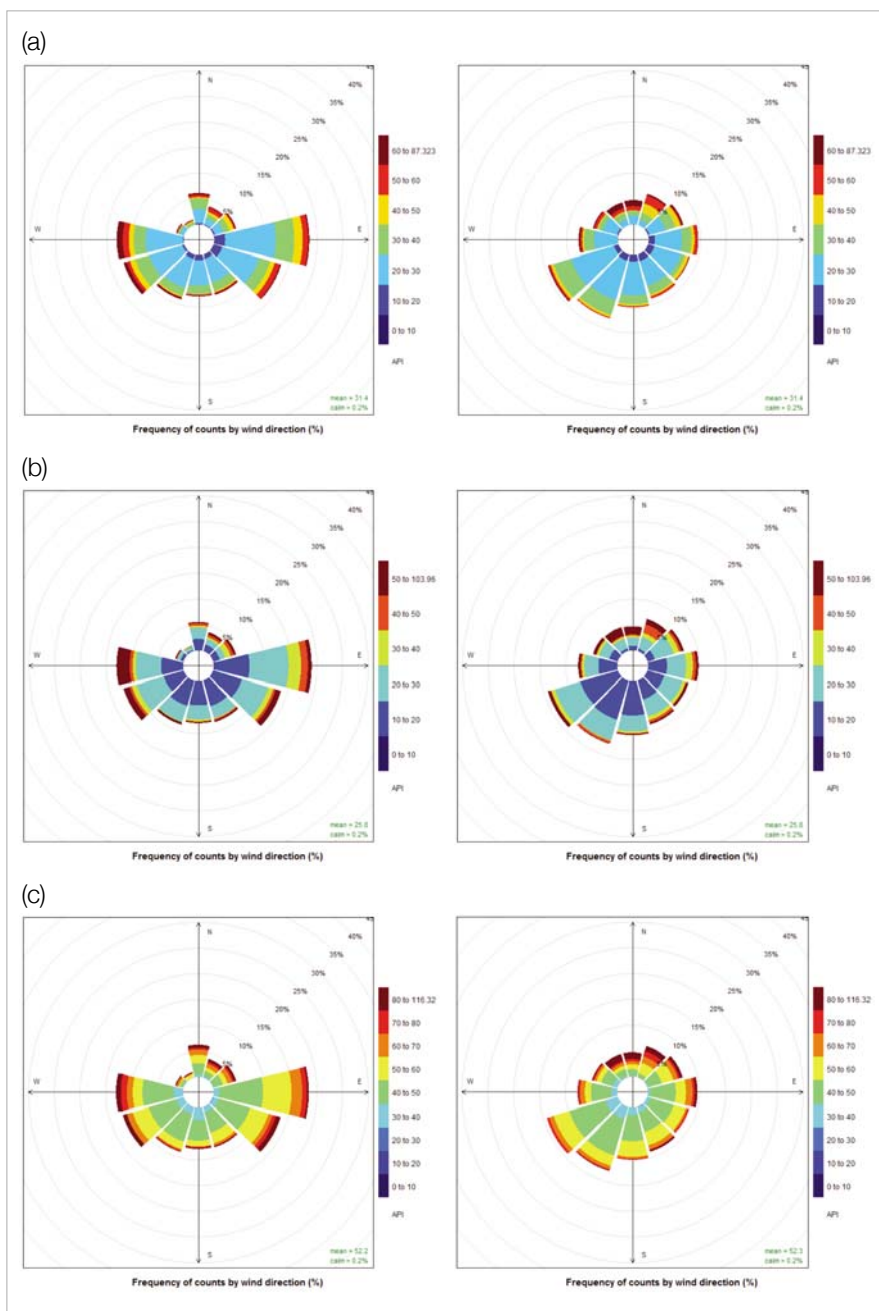


Figure 24. Pollution rose of the API averaged over a) general stations, b) Tap Mun station, and c) roadside stations in Hong Kong during JJA 2000–2009 at 100 m and 1500 m elevation.

Reference:

Chow, E. C. H., R. C. Y. Li and W. Zhou, 2015: Synoptic weather control of summer air quality in Hong Kong. Submitted to Aerosol and Air Quality Research. (under review)

C6. Intraseasonal variation of visibility in Hong Kong

(PI: Wen ZHOU)

Visibility is one of the parameters for indicating air pollution. Associated with the intraseasonal variation of different environmental parameters, an obvious variation in visibility impairment is found in both summer and winter. In summer, local visibility and air quality are found to be significantly affected by the intraseasonal oscillation (ISO) through modulation of associated atmospheric circulations. In winter, the modulation effects appear to be weaker due to the southward shift of the ISO-related convection (Figure 25). For more details, please refer to Zhou et al. (2015).

In summer, local visibility and air quality are found to be significantly affected by the intraseasonal oscillation through modulation of associated atmospheric circulations.

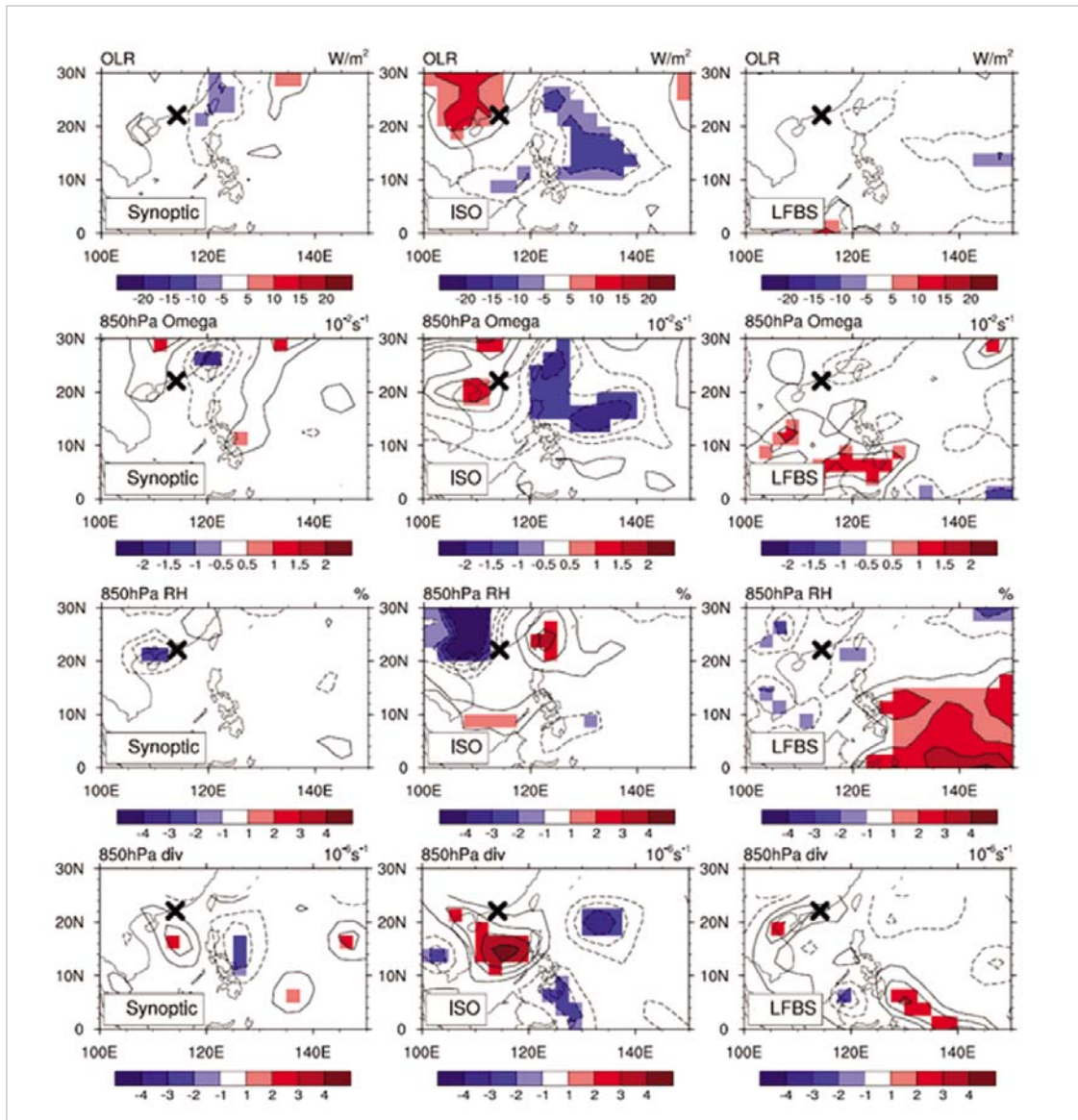


Figure 25. Composites of the synoptic (left panel), intraseasonal (middle panel), and LFBS (right panel) components of outgoing long-wave radiation (W/m^2), 850-hPa omega ($10^{-2} s^{-1}$), 850-hPa relative humidity (%), and 850-hPa divergence ($10^{-6} s^{-1}$) associated with visibility impairment in Hong Kong during summer. Shading and colored vectors denote anomalies that are over 90% confidence, and the crosses denote the position of Hong Kong.

Reference:

Zhou, W., C. Y. Li and C. H. Chow, 2015: Intraseasonal variation of visibility in Hong Kong. Submitted to *Advances in Atmospheric Sciences*. (under review)

Publications

Journal Papers

- An, K. J., Y. F. Lam, S. Hao, T. E. Morakinyo and H. Furumai, 2015: Multi-purpose rainwater harvesting for water resource and the cooling effect. *Water Research*, **86**, 116-121, doi: 10.1016/j.watres.2015.07.040.
- Chan, K. L., S. Y. N. Jiang and Z. Ning, 2016: Speciation of water soluble iron in size segregated airborne particulate matter using LED based liquid waveguide with a novel dispersive absorption spectroscopic measurement technique. *Analytica Chimica Acta*, **914**, 100-109.
- Cheung, H. H. N. and W. Zhou, 2015: Implications of Ural blocking for East Asian winter climate in the CMIP5 models. Part I: Biases in the historical scenario. *J. Climate*, **28**, 2203-2216, doi: 10.1175/JCLI-D-14-00308.1.
- Cheung, H. H. N. and W. Zhou, 2015: Implications of Ural blocking for East Asian winter climate in the CMIP5 models. Part II: Projection and uncertainty in future climate conditions. *J. Climate*, **28**, 2217-2233, doi: 10.1175/JCLI-D-14-00309.1.
- Cheung, H. H. N., W. Zhou, S. M. Lee and H. W. Tong, 2015: Interannual and interdecadal variability of the number of cold days in Hong Kong and their relationship with large-scale circulation. *Mon. Wea. Rev.*, **143**, 1438-1454, doi 10.1175/MWR-D-14-00335.1.
- Kun, H. Y., C.-Y. Tam, W. Zhou and S.-J. Sohn, 2015: Seasonal prediction of June rainfall over South China: Model assessment and statistical downscaling. *Adv. Atmos. Sci.*, **32**, 680-689, doi: 10.1007/s00376-014-4047-x.
- Leung, M. Y.-T., H. H. N. Cheung and W. Zhou, 2015: Energetics and dynamics associated with two typical mobile trough pathways over East Asia in boreal winter. *Clim. Dyn.*, **44**, 1611-1626, doi: 10.1007/s00382-014-2355-6.
- Leung, M. Y.-T. and W. Zhou, 2015: Vertical structure, physical properties and energy exchange of the East Asian trough in boreal winter. *Clim. Dyn.*, **45**, 1635-1656, doi: 10.1007/s00382-014-2419-7.
- Leung, M. Y.-T. and W. Zhou, 2015: Variation of circulation and East Asian climate associated with anomalous strength and displacement of the East Asian trough. *Clim. Dyn.*, **45**, 2713-2732, doi:10.1007/s00382-015-2504-6.
- Li, Y., K. K. W. Cheung and J. C. L. Chan, 2015: Modeling the effects of land-sea contrast on tropical cyclone precipitation under environmental vertical wind shear. *Quart. J. Roy. Meteor. Soc.*, **141**, 396-412.
- Li, R. C. Y. and W. Zhou, 2015: Interdecadal changes in summertime tropical cyclone precipitation over Southeast China during 1960-2009. *J. Climate*, **28**, 1494-1509, doi: 10.1175/JCLI-D-14-00246.1.
- Li, R. C. Y. and W. Zhou, 2015: Multiscale control of summertime persistent heavy precipitation events over South China in association with synoptic, intraseasonal, and low-frequency background. *Clim. Dyn.*, **45**, 1043-1057, doi: 10.1007/s00382-014-2347-6.
- Li, R. C. Y., W. Zhou and T. C. Lee, 2015: Climatological characteristics and observed trends of tropical cyclone-induced rainfall and their influences on the long-term rainfall variations in Hong Kong. *Mon. Wea. Rev.*, **143**, 2192-2206, doi: 10.1175/MWR-D-14-00332.1.
- Li, X. Z., W. Zhou and Y. Q. Chen, 2015: Assessment of regional drought trend and risk over China: A drought climate division perspective. *J. Climate*, **28**, 7025-7037.
- Lin, I.-I. and J. C. L. Chan, 2015: Recent decrease in tropical cyclone destructive potential in the western North Pacific Ocean. *Nature Comm.*, doi: 10.1038/ncomms8182.

- Moon, I.-J., S. H. Kim, P. Klotzbach and J. C. L. Chan, 2015: Roles of interbasin frequency changes in the poleward shifts of the maximum intensity location of tropical cyclones. *Environ. Res. Lett.* **10** 104004, doi:10.1088/1748-9326/10/10/104004.
- Morakinyo, T. E. and Y. F. Lam, 2015: Simulation study of dispersion and removal of particulate matter from traffic by road-side vegetation barrier. *Environmental Science and Pollution Research*, doi: 10.1007/s11356-015-5839-y.
- Qian, C., W. Zhou, S. K. Fong and K. C. Leong, 2015: Two approaches for statistical prediction of non-Gaussian climate extremes: A case study of Macao hot extremes during 1912-2012. *J. Climate*, **28**, 623-636, doi:10.1175/JCLI-D-14-00159.1.
- Sun, L., K. C. Wong, P. Wei, S. Ye, H. Huang, F. Yang, D. Westerdahl, P. K. K. Louie, C. W. Y. Luk and Z. Ning, 2016: Development and application of a next generation air sensor network for the Hong Kong marathon 2015 air quality monitoring. *Sensors (Switzerland)*, **16 (2)**, 18 p.
- Wang, L., W. Chen, W. Zhou and G. Huang, 2015: Drought in Southwest China: A review. *Atmos. Oceanic Sci. Lett.*, **8**, 339-344, doi: 10.3878/AOSL20150043.
- Wang, L., W. Chen, W. Zhou and G. Huang, 2015: Teleconnected influence of tropical Northwest Pacific Sea surface temperature on interannual variability of autumn precipitation in Southwest China. *Clim. Dyn.*, **45**, 2527-2539, doi: 10.1007/s00382-015-2490-8.
- Wang, W. W., W. Zhou, S. K. Fong, K. C. Leong, I. M. Tang, S. W. Chang and W. K. Leong, 2015: Extreme rainfall and summer heat waves in Macao based on statistical theory of extreme values. *Climate Research*, **66**, 91-101.
- Williamson, F., R. Allan, A. D. Switzer, J. C. L. Chan, R. J. Wasson, R. D'Arrigo and R. Gartner, 2015: New directions in hydro-climatic histories: Observational data recovery, proxy records and the Atmospheric Circulation Reconstructions over the Earth (ACRE) initiative in Southeast Asia. *Geosci. Lett.*, doi: 10.1186/s40562-015-0018-z.
- Xia, J. J., Z. W. Yan, G. S. Jia, H. Q. Zeng, Philip Joes, W. Zhou and A. Z. Zhang, 2015: Projections of advance the start of growing season during the 21st century based on CMIP5 simulations. *Adv. Atmos. Sci.*, **32**, 831-838, doi: 10.1007/s00376-014-4125-0.
- Xia, J. J., Z. W. Yan, W. Zhou, S. K. Fong, K. C. Leong, I. M. Tang, S. W. Chang, W. K. Leong and S. F. Jin, 2015: Projection of the Pearl River Delta's potential submerged area due to sea level rise during the 21st century based on CMIP5 simulations. *Acta Oceanologica Sinica*, **34**, 78-84.

Staff list

Director

Prof. Johnny CHAN Chair Professor of Atmospheric Science

Deputy Director

Dr. Zhi NING Assistant Professor

Members

Prof. Ronghui HUANG Honorary Professor (Academician, Chinese Academy of Sciences)

Prof. Chongyin LI Honorary Professor (Academician, Chinese Academy of Sciences)

Prof. Peter BRIMBLECOMBE Associate Dean (Research and Postgraduate Studies)

Chair Professor of Environmental Chemistry

Dr. Wen ZHOU Associate Professor

Dr. Nicky LAM Assistant Professor

Dr. Keith NGAN Assistant Professor

Advisory Committee

Prof. Yihui DING Academician, Chinese Academy of Engineering

Lord Prof. Julian HUNT Professor, University College London, Fellow of Royal Society

Researchers

Appointed by Centre

Dr. Frederick Dane WESTERDAHL Research Fellow

Dr. Tao FENG Postdoctoral Fellow

Dr. Agata Barbara RAKOWSKA Senior Research Associate

Dr. Ho Nam CHEUNG Senior Research Assistant

Mr. Kin Sik LIU Senior Research Assistant

Mr. Chak Hang CHOW Research Assistant

Mr. Jiapeng LIU Research Assistant

Ms. Li SUN Research Assistant

Ms. Xinxin ZHANG Research Assistant

Guy Carpenter Asia-Pacific Climate Impact Centre
City University of Hong Kong
Tat Chee Avenue, Kowloon,
Hong Kong, China.

Tel: (852) 3442 7359

Email: gcacic@cityu.edu.hk

Website: <http://www.cityu.edu.hk/gcacic/>



Printed on FSC™ Certified Paper with SOY INK

